Composites: Part A 156 (2022) 106902

Contents lists available at ScienceDirect

Composites Part A

journal homepage: www.elsevier.com/locate/compositesa

Additive binding layers to suppress free edge delamination in composite laminates under tension

Miguel Ubago Torres [a,*], Meisam Jalalvand [b]

[a] Department of Mechanical and Aerospace Engineering, University of Strathclyde, 75 Montrose Street, Glasgow G1 1XQ, UK
[b] Engineering Materials, Faculty of Engineering and Physical Sciences, University of Southampton, Southampton SO17 1BJ, UK

ARTICLE INFO

Keywords:
Finite Element Analysis (FEA)
Failure
Angle-ply
Mechanical testing

ABSTRACT

An additive laminate applied to the free-edges of composite laminates is proposed to stop the development of delamination. Numerical analyses were conducted to find the optimum additive binding layup and the experimental results proved that the free-edge delamination was successfully suppressed. When it was used to bind the edges of a $[(20_2/-20_2)_2]_s$ angle-ply laminate, the tensile failure strain and load of the laminate were increased by about 50%, and the failure mode changed from free-edge delamination to in-plane shear. However, it did not change the failure load and final failure mode of a $[45_2/0_2/-45_2/90_2]_s$ quasi-isotropic laminate, as this substrate is less susceptible to free-edge delamination. Thus, this technique is an efficient solution for suppressing free-edge delamination in real structural applications and in the characterisation of coupon tests where damage at the free-edges undermines the real potential of the composite substrate.

1. Introduction

Delamination at the free edges is one of the important damage modes in composite laminates that occurs as a result of interlaminar stresses that arise at free-edges [1]. It reduces the stiffness and strength of the laminates, leading to significant structural integrity loss and eventually laminate failure. Additionally, free-edge delamination is a significant problem for the testing and characterisation of laminated composites. Unlike most final composite products, which have no or a small number of free-edges, test coupons have long free-edges that make them susceptible to free-edge delamination. This undermines the actual load-bearing capacity of the laminate and gives non-representative test results.

Given its importance, free-edge delamination has been studied for decades, and relatively good explanations and reliable methods to predict its development have been proposed. A full three-dimensional stress distribution in composite laminates under axial extension was first given by Pipes and Pagano [2]. This work led to numerous investigations [3–8] on the effect of the free-edges from the stress analysis perspective. These studies demonstrated that interlaminar through-thickness stress σ_z (see Fig. 1 for sign convention) and shear stress τ_{xz} are maximum, approaching infinity, at the free-edge. In contrast, the shear stress τ_{yz} is maximum close to the edge but zero at the edge. Due to such stress singularity at the edges, alternative methods for studying and predicting free-edge delamination were needed.

Rybicki et al. [9] were the first to model the initiation and stable crack growth of delamination using the interlaminar energy release rate (G). O'Brien [10] used this approach to characterise the onset and development of delamination based on the energy release rate and classical laminate theory. Furthermore, Wang [11] studied the influence of fibre orientation, crack length, and ply thickness on free-edge delamination using stress intensity factors and energy release rate. He showed that the mode-III stress intensity factor is one or two orders of magnitude higher than mode-I and mode-II stress intensity factors in angle-ply laminates. Ye [12] studied the role of the matrix on delamination, proposing a strength criterion for the onset of delamination based on the matrix properties. The results showed that critical loads for the onset of delamination could be increased by means of enhancing matrix strength and ductility for laminates under static loading.

Two different groups of approaches to delay or suppress the initiation and growth of free-edge delamination have been investigated:

(1) Solutions suggesting laminate modification, e.g. Chan and Wang [13] used a *hybridisation* solution, replacing one of the carbon/epoxy plies in the original laminate with a lower stiffness glass/epoxy ply, achieving higher loads before the onset of

* Corresponding author.
E-mail address: miguel.ubago-torres@strath.ac.uk (M. Ubago Torres).

https://doi.org/10.1016/j.compositesa.2022.106902
Received 21 December 2021; Received in revised form 22 February 2022; Accepted 25 February 2022
Available online 1 March 2022

delamination and final failure. Similarly, the *interleaving* [14] technique places a discrete layer of tough unreinforced resin between the layers to achieve a higher interlaminar fracture toughness.

(2) Solutions that apply a local modification at the free edges to increase their interlaminar strength, e.g., Lackman and Pagano [15] experimentally demonstrated that serrating the free-edges of the laminate can reduce the chance of delamination. In layups including 90-degree layers, the Poisson's ratio of the 90-degree ply relative to other ply orientations is a primary source of increased local stresses. The *critical ply termination* [16] technique ends the 90-degree ply a small distance away from the free-edges, and the *discrete critical ply* [17] technique proposes segmenting the 90-degree ply in the width direction so the loading path for delamination growth is interrupted. Mignery et al. [18] proposed a *stitching* technique that effectively arrested delamination but decreased the tensile strength of the laminate. In 1989, Howard et al. [19,20] presented a U-shaped cap as a reinforcement for free-edges. A stress analysis at the edges and a qualitative semi-empirical correlation was carried out, showing reduction of the interlaminar stresses at the free-edges of a $(30_2/-30_2/90_3/-30_2/30_2)$ carbon/epoxy laminate. More recently, Chuaqui et al. [21,22] have presented an effective resin treatment on free edges to improve the short beam shear test accuracy and avoid free-edge delamination while simulating several non-standard layups in open hole laminates under tension. This technique bonds two resin blocks onto the free edges of the laminate, reducing the interlaminar stresses and delaying the onset and propagation of delamination.

In this paper, an additive composite laminate made out of thin-ply unidirectional prepregs is applied to the free-edges of cured composite laminates to suppress free-edge delamination, as schematically shown in Fig. 1. In this paper, these thin secondary added composite layers are referred to as "additive binding" as they are added to the main substrate and cured in a second stage to bind the layers together at the free edges. The applied method is similar to what was proposed by Howard et al. [19,20], where they highlighted the need for a suitable method for accounting for delamination as the stress-based method they used was mesh-sensitive due to the singularity around the free-edges, and the presence of delamination could not be modelled. To address this issue, the effect of additive binding is studied on the energy release rates at the presence of different delamination sizes and locations using the virtual crack closure technique (VCCT) [23]. The developed technique is used to study a wide range of additive binding layups. As will be presented, a different optimum layup is suggested as opposed to that proposed in [19,20]. This study shows that bindings can suppress the growth of free-edge delamination as it propagates to larger sizes by reducing the energy release rates. Also, the thermal analysis done in the paper shows that the bindings will not introduce any opening tensile or extra shear stress, so they do not negatively compromise the strength of the laminate.

Additionally, the recent developments in the tow spreading techniques and thin-ply technology [24] have allowed the introduction of small amounts of additive secondary materials in the experiments. This provides the opportunity to suppress the free-edge delamination with a minimal alteration of the geometry, significantly less than those that used standard ply thickness materials, e.g., those by Howard et al.

It will be shown that this solution can achieve more realistic and precise composite strength characterisation results by eliminating the free-edge delamination where this damage mode causes premature failure. Additionally, in industrial applications which include free-edges, this solution can efficiently improve the composite strength by suppressing or delaying delamination.

The proposed solution is studied on two different composite substrate layups: (1) $[(20_2/-20_2)_2]_s$ angle-ply layup susceptible to developing free-edge delamination, and (2) $[45_2/0_2/-45_2/90_2]_s$ quasi-isotropic layup that is less significantly affected by free-edge delamination. The two substrate laminates $[(20_2/-20_2)_2]_s$ and $[45_2/0_2/-45_2/90_2]_s$ will be identified as Angle-Ply (AP) and Quasi-Isotropic (QI) laminates, hereafter.

Additionally, the effect of the binding was studied experimentally. The obtained results indicate that damage modes triggered by free-edge, e.g., delamination and matrix cracking, can be successfully suppressed using this technique, whereas other damage modes are not affected.

2. Concept

Due to the low strength of the polymer matrices, interlaminar cracks known as delamination can develop between the layers, as illustrated in Fig. 1a. The fundamental concept of the solution proposed in this paper is a new thin-ply laminate applied in a second curing stage to the free edges of a composite substrate. This laminate acts as a binding, providing constraint and holding the plies of the substrate together, as illustrated in Fig. 1b. This binding can introduce fibre reinforcement in the thickness direction at the free-edges, and therefore, it enhances the interlaminar strength of the laminate around the free edges. It also constrains relative out-of-plane and shear movements of different plies at the free edge, reducing the risk of delamination.

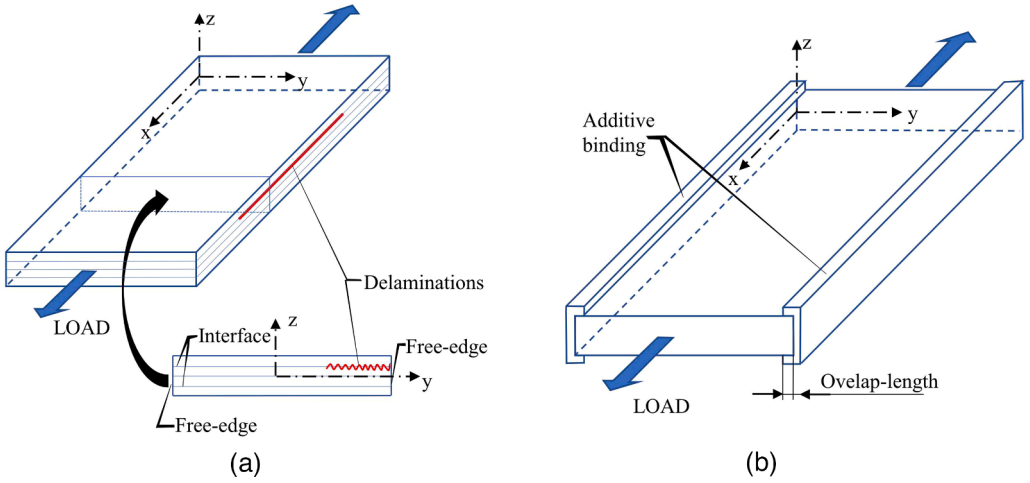

Fig. 1. A composite laminate subjected to axial load. (a) No binding applied with free-edge delamination, (b) additive binding applied at the free edges. (For interpretation of the references to colour in this figure legend, the reader is referred to the web version of this article.)

3. Analysis and specimen design

3.1. Substrate laminate selection

A layup susceptible to free-edge delamination, when subjected to axial loading, is sought to study the effectiveness of the additive binding solution. The substrate laminate is chosen to be balanced and symmetric to avoid coupling effects. Different stacking sequences of $[\pm\theta]_s$, with θ between 0 and 90 degrees were studied. Eq. (1) presented in Appendix I of O'Brien's paper [10] was used to find the energy release rate at the free edges for different laminates. It is worth mentioning that O'Brien provides another version of this equation, in the same paper, with 2 in the denominator instead of 4 and justifies that for laminates with matrix cracking in central 90-degree layers and a zig-zag shape of the delamination. As there is no 90-degree layer in the assumed $[\pm\theta]_s$ laminates to link the delaminations at different interfaces Equation 1 is deemed to be more accurate, and as will be explained in Section 3.2 Finite element analysis, this version of the equation gives relatively close results to the Finite Element (FE) predictions.

$$G = \frac{\varepsilon^2 t}{4}(E_{lam} - E^*) \tag{1}$$

where G is the strain energy release rate, ε is the nominal applied strain, t is the total thickness of the laminate, E_{lam} is the engineering Young modulus of the laminate, and E^* is the engineering Young modulus of the laminate completely delaminated along one or more interfaces. Fig. 2 displays the variation of the energy release rate for the $[\pm\theta]_s$ layups versus θ using Eq. (1). The material properties used for the laminate are those presented in Table 1 for IM7/913 carbon/epoxy composite, along with the nominal ply thickness of 0.13 mm and the applied strain of $\varepsilon = 1\%$.

The value of G is maximum for values of θ around 16 degrees. For this study, θ is selected to be equal to 20 degrees. This angle-ply layup still gives a high G value, and its susceptibility to free-edge delaminate has been studied and reported by Xu and Wisnom in [25]. Additionally, we know that the energy release rate is proportional to the ply block thickness. Therefore, the stacking sequence $[(20_2/-20_2)_2]_s$ is selected as a substrate laminate susceptible to free-edge delamination. A quasi-isotropic laminate with the stacking sequence of $[45_2/0_2/-45_2/90_2]_s$ is also selected to study the effect of the additive binding on laminates not sensitive to free-edge delamination. This layup is similar to the one studied by O'Brien in [26], so it is expected to indicate matrix cracking in the off-axis layers followed by local free edge delamination before the final failure due to failure of the 0 layers.

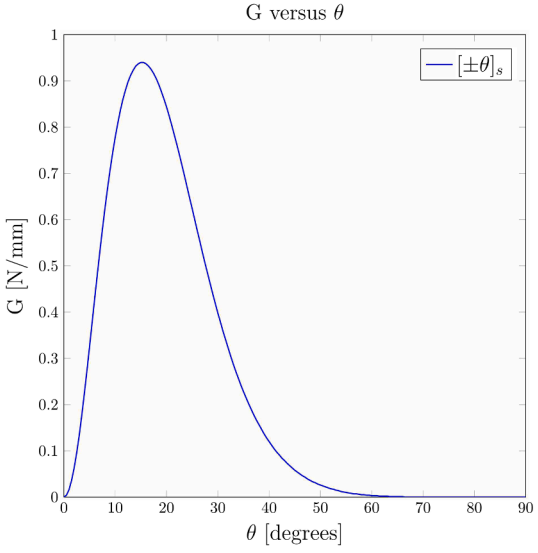

Fig. 2. Variation of energy release rate (G) for free edge delamination in $[\pm\theta]_s$ angle-ply layups versus θ using Equation 1 from O'Brien Appendix I [10]. (For interpretation of the references to colour in this figure legend, the reader is referred to the web version of this article.)

3.2. Finite element analysis

A Python code was developed for Abaqus 2019 to carry out several numerical simulations automatically. The code was built for calculating the energy release rate values at the crack tip in the substrate laminate when subjected to axial strain. Simulations were performed on both AP and QI laminates to study the effect of length and position (interface number) of the interlaminar crack on the energy release rate. In each layup, the interfaces with the highest energy release rate values are those assumed to fail before the others and are referred to as the *critical interfaces*. The energy release rates at the critical interfaces of the models with and without bindings are compared to study the effect of the additive bindings to suppress delamination. The energy release rates are calculated using the nodal forces and displacements at the crack tip and neighbouring nodes in three directions, according to [23]. The VCCT was used to calculate the energy release rate in modes I, II, III. Finally, the total energy release rate was calculated according to Eq. (2). It is worth mentioning that the VCCT provides a good insight on cases dominated by free-edge delamination as their main failure mode. For other cases, especially for failure modes interacting with each other, more than one crack might be necessary to model and one may prefer to use progressive damage analysis. The aim of this paper is to provide insight on which binding laminate gives the best results for stopping free-edge delamination. Hence, to model several different binding layups and find the optimum one, the VCCT offers a few advantages over other techniques, e.g., progressive damage modelling using cohesive elements: (i) it is fast and numerically efficient, (ii) it directly provides G values, so makes comparing the efficiency of different bindings straightforward.

$$G = G_I + G_{II} + G_{III} \tag{2}$$

The finite element model presented is applicable to any layup, independent of its ply thickness, width, ply orientation, etc. The model assumes presence of a delamination crack so the value of G can be calculated at the crack tip using VCCT. The finite element model of the composite substrate was built using individual layers meshed with 3D-8noded brick elements (C3D8I). Each layer of the substrate and additive binding had a mesh size of 0.05 mm in the width (Y) direction (see Fig. 3). Also, two elements per ply thickness for both substrate and the binding and two elements in the length (X) direction was used. The stress field does not vary along the length of the specimen at points distant from the end tabs, and therefore, a generalised plane strain condition is applicable as explained by Pipes and Pagano in [2]. This will give accurate stress and strain field at points in the middle of the sample and significantly reduce the computational cost. A slice model, as proposed by Jiang [27], based on the generalised plane strain condition, was used instead of a full tensile sample model, as shown schematically in Fig. 3a. The aim of the generalised plane strain is to mimic the displacement field far away from the end tabs, where the displacement field is constant at different sections. It is worth mentioning that variation of displacement across a section is expected away from the tabs

and the slice in Fig. 3 is correctly seen to be slightly deformed out of plane. However, this displacement field stays the same for different slices far from the end tabs. The substrate slice models are 20 mm wide, 0.07 mm long, and 2.08 mm thick. The binding dimensions used are 0.03 mm per ply thickness and an overlap length of 5 mm. Only one crack on one side of the layup was modelled, making the slice model asymmetrical. This is because the interlaminar cracks on both edges are independent of each other, and the lack of delamination on one side does not change the G values on the other side. Fig. 3b shows the slice finite element model with the additive binding applied. The substrate laminate represented in Fig. 3b shows a 4.5 mm long edge-delamination at interface 1 between the first block of 20 and −20 degree plies of the AP laminate (see Fig. 4 for reference).

The generalised plane strain condition is achieved by applying equation-type restrictions to node pairs with equal y and z coordinates on either side of the slice. All nodes on one face of the slice are constrained to have the same displacements, in the transverse (v) and thickness (w) directions, as that of their equivalent nodes on the opposite face. For example, points M and M', opposite nodes on the front and back faces, as shown in Fig. 3, are constrained as below:

$$v_M - v_{M'} = 0 \tag{3}$$

$$w_M - w_{M'} = 0 \tag{4}$$

Another constraint should be applied to guarantee uniform longitudinal strain on the loading direction. This is achieved by fixing the distance between the corresponding nodes, e.g., M and M', proportional to the applied extension, $\varepsilon = 1\%$, and the slice length L in the loading direction as shown below:

$$u_M - u_{M'} = \varepsilon L \tag{5}$$

where u represents the movement of each node in the loading direction, as shown in Fig. 3b. A minimum of two elements in the loading direction is required to avoid any interference of the constraining equations or reaction forces on the back and front faces with the nodal forces used in VCCT. This will allow the node at the midplane of the slice model not to be directly constrained by equations [3–5] and be used to calculate the energy release rate values at the crack tip. The layers of the substrate laminate were constrained together using the tie function in Abaqus. The layers adjacent to the pre-crack were constrained together with a surface-to-surface contact interaction with a small sliding formulation and surface-to-surface discretisation. Arbitrary high values of fracture toughness equal to $9{\cdot}10^{34}$N/mm were applied to avoid crack growth simulation. Delamination growth is not aimed to be modelled, as the focus of this study is to compare the impact of the additive binding on the energy release rate at different interfaces and crack lengths.

The free-edges of the substrate laminate were not tied to the internal surface of the binding laminates, as seen in Fig. 3b. This is to consider the possibility of unbonded additive binding layers to the free edges of the substrate and obtain conservative upper limit energy release rates for the cases with additive binding. To study the possibility of a crack occurring between the top/bottom surface of the binding and the substrate, models with initial cracks were simulated on the AP substrate laminate. The value of G at the crack between the binding and the substrate laminate was found to be insignificant, less than 2.5% of the maximum value of G at the critical interface of the same substrate. Therefore, no delamination is expected between the binding and the substrate, and the additive bindings were tie-constrained to the substrate's top and bottom surfaces and tie constrained among themselves. In this way, no cracks were considered between the top and bottom surfaces of the substrate laminate and the additive binding.

Different crack lengths at three interfaces between layer blocks with different fibre orientations were modelled due to the symmetry of the laminates. Fig. 4 shows the total energy release rate (G) variation for different pre-crack lengths for the AP and QI laminates obtained from the slice FE model. For the AP laminate, the critical interface is interface 1. In the QI laminate case, the critical interface is interface 3. Therefore, these interfaces are most likely to delaminate at the free-edges. The run time for each simulation was approximately 5 min for each delamination length. This short simulation time, along with the applied fine element size were possible as the slice modelling technique was used.

Fig. 4 also shows the G values calculated using Equation 1 for the critical interfaces. The material properties used are those in Table 1. E^* was calculated assuming AP laminates totally delaminate at interfaces 1 and its symmetric equivalent. Similarly, QI laminates were assumed to be totally delaminated at interfaces three and its symmetric equivalent when calculating E^*. (see Fig. 4 for interface numbers reference). Eq. (1), proposed by O'Brien, seems to have a relatively acceptable agreement with the asymptote of the FE results given its simplicity and ease of application.

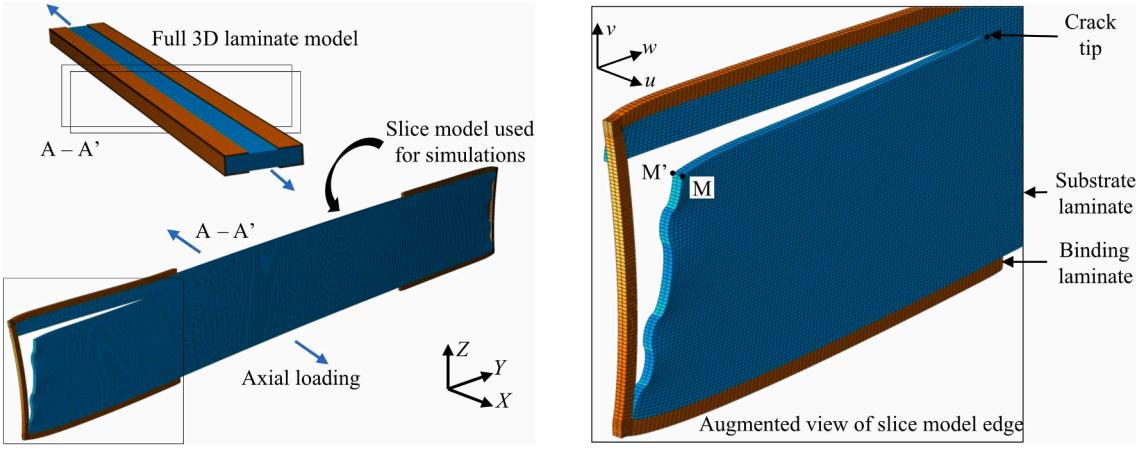

Fig. 3. Slice model based on generalised plane strain condition with an additive binding. (a) Figure of the slice model used for the simulation, taken from the centre of a full 3D model representation (not used in the simulations), (b) details of a free-edge delamination model with an additive binding. (For interpretation of the references to colour in this figure legend, the reader is referred to the web version of this article.)

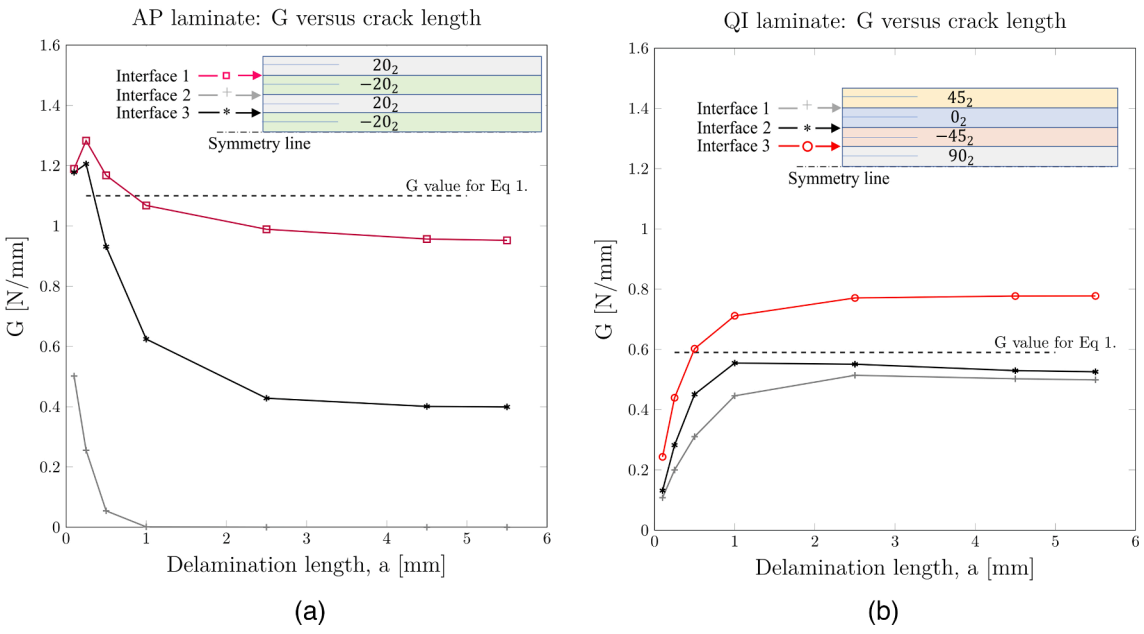

Fig. 4. Energy release rate for interlaminar cracks at different crack lengths and interfaces for an applied strain of 1%. (a) AP laminate, (b) QI laminate. (For interpretation of the references to colour in this figure legend, the reader is referred to the web version of this article.)

As shown in Fig. 4, the longest crack length simulated is 5.5 mm, which is a relatively big crack size for a total laminate width of 20 mm. As the crack length increases, the stiffness of the substrate and, consequently, the G value can reduce (see Eq. (1)). The change in the stiffness is only 2.5% from a 0.1 mm crack length to a 5.5 mm crack length in the AP laminate. Therefore, the application of a constant strain (displacement control) rather than constant stress (load control) is not expected to affect the results shown above. Additionally, similar stiffness reduc-

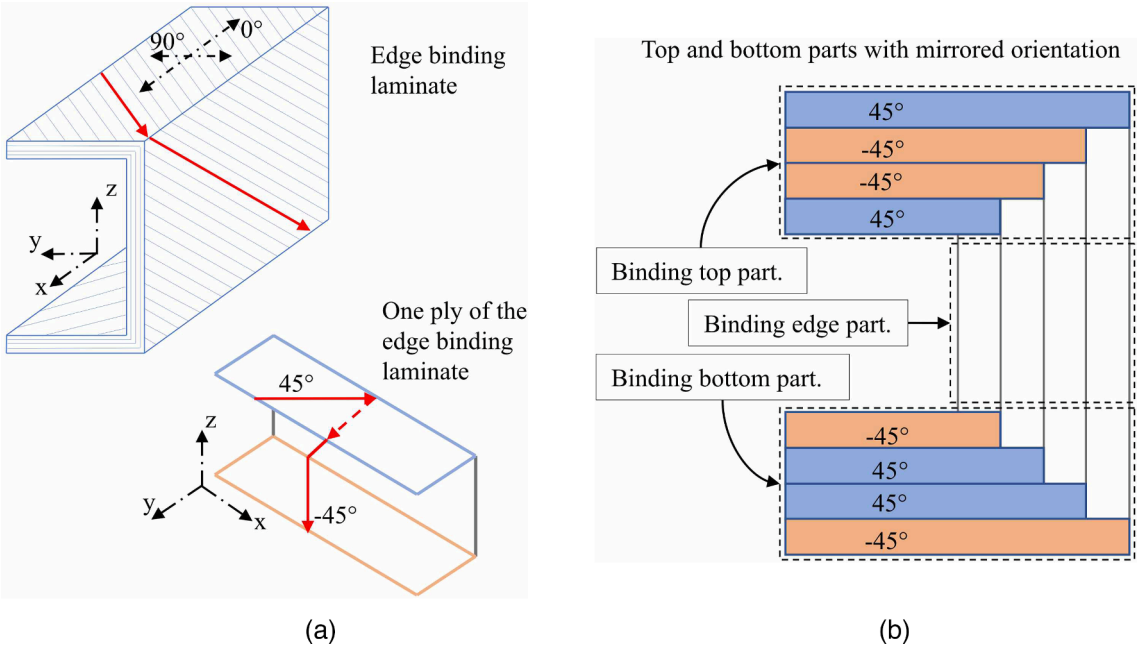

Fig. 5. Change of the fibre orientation in the binding. (a) Fibre direction in a multi-layer edge binding and in one of the edge binding plies, (b) top and bottom parts of the binding with mirrored orientation. (For interpretation of the references to colour in this figure legend, the reader is referred to the web version of this article.)

tion occurs in the model with the binding, so both models with and without binding under displacement control are directly comparable, and the stiffness reduction due to increased crack length does not compromise such comparison. The FE model is linear-elastic, and for ease of analysis and comparison, all simulations are performed with 1% applied strain. The energy release rate at different strains is quadratically proportional and can be calculated straight away.

3.3. Binding design

When the uncured flat binding laminate made out of thin-ply unidirectional prepreg is bent over the substrate laminate edges (see section 4.2. *Specimens manufacture.* for the specimen's manufacture method), its fibre orientation in the top part (see Fig. 5b for reference) inverts in the binding bottom part. In other words, each layer orientation of the binding in the top part is mirrored in the bottom part. Fig. 5 shows a schematic representation of the binding's layup and its stacking sequence on the top and bottom parts. It was decided to have a symmetrical and balanced additive binding layup to minimise any coupling effects between the in-plane tension and other deformation modes. While the whole binding is not perfectly symmetric versus the substrate midplane, it is relatively close to being symmetric and given its small dimensions compared to the main substrate, the bending-tension coupling is expected to be negligible.

A large number of simulations were performed looking for the best binding layup. Different additive binding layups were tried for minimising the energy release rate at the critical interfaces using numerical analysis explained in Section 3.2 *Finite element analysis.* Both AP and QI laminates are symmetric and therefore have two critical interfaces symmetric against the mid-plane. For the AP laminate, the critical interfaces are interface number 1 and 7, indicated by // in the layup ($[20_2//-20_2/20_2/-20_2/-20_2/20_2/-20_2//20_2]$). In the case of the QI laminate, interfaces 3 and 5 are the critical interfaces in the layup ($[45_2/0_2/-45_2//90_2/90_2//-45_2/0_2/45_2]$). As shown in Fig. 4, in both AP and QI cases, after delamination lengths of about 4 mm, the energy release rate values follow a constant asymptotic value. Therefore, a pre-crack of 4.5 mm was modelled at the critical interface of the AP and QI substrate laminates. Different additive bindings with stacking sequence of $[\pm\theta]_s$,$[\theta]_4$ and $[\theta/\varphi]_s$ were numerically analysed, with φ changing from 0 to 90 degrees with 15 degrees intervals, and θ changing from −90 to 90 degrees with 15 degrees intervals for each φ angle. The total energy release rate (G) results of these simulations are presented in Fig. 6(a) and (b). For each layup, the presence of the 4.5 mm pre-crack at either of the critical interfaces of the AP and QI laminates was studied, and the higher value is reported in Fig. 6, so the effect of the binding asymmetry is considered in the results.

According to the results shown in Fig. 6, the $[\pm45]_s$ layup is the optimum binding layup that gives the minimum energy release rate for the AP substrate. This binding layup reduces the energy release rate value by around 70%, from 0.94 to 0.28 N/mm.

Different binding layups for the QI substrate laminate have a minor impact on reducing the total energy release rate value. For comparison with the AP substrate laminate, a $[\pm45]_s$ binding layup was chosen for the QI laminate experiments. This layup reduces the energy release rate by 19%, from 0.78 to 0.63 N/mm. Different binding layups give similar G values. The $[0]_4$ and $[90]_4$ binding layups only have one fibre orientation, so they are easier to manufacture. The $[0]_4$ gives the G value of 0.63 N/mm for the QI laminate case, which reduces 22% compared with the substrate without binding, and it is lower than the value of G given by $[90]_4$ binding layup. Hence, the $[0]_4$ binding layup was also selected for additional testing on the effectiveness of the additive bindings.

The comparison of the energy release rate values for different delamination lengths at the critical interfaces with a $[\pm45]_s$ binding against laminates without binding is shown in Fig. 7a and b for the AP and QI substrates, respectively.

The AP laminate with a $[\pm45]_s$ additive binding still presents high G values for small edge delaminations (Fig. 7a). However, as the delamination grows, the value of G reduces rapidly, indicating that the crack propagation would be suppressed by the binding. For the QI laminate with a $[\pm45]_s$ binding, shown in Fig. 7b, the value of G is less reduced and stays just under the G values for QI laminate without binding for different delamination lengths.

Separate simulations were carried out to determine the effect of the binding overlap-length over the substrate laminate width (see Fig. 1b for the definition of overlap length). Fig. 8 indicates the variation of energy release rate versus the binding overlap-length for a $[\pm45]_s$ additive binding layup, with different delamination lengths at interface 1 of the AP laminate. Numerically, small binding overlap-length have a similar effect to those bindings with longer overlap-length. This is because the binding overlapping part does not significantly contribute to load transfer and the constraining of the delamination. Therefore, for the experiments, the binding overlap-length was decided to be 5 mm, allowing repeatability in the manual manufacture process of the laminate with binding (see specimens manufacture process in 4.2).

3.4. Thermal effects

In this section, it will be shown that the residual stresses induced by the bindings will not have a negative impact on the free-edge stress state in both layups and that the bindings will induce a small compressive through-thickness direction residual stresses to the substrate laminate, which can have a small positive impact to suppress delamination.

Coefficients of thermal expansion used for IM7/913 are $\alpha1 = -9 \times 10^{-7}$ 1/K and $\alpha2 = \alpha3 = 2.88 \times 10^{-5}$ 1/K taken from [28]. For TC33/K51, the estimated thermal expansion coefficients from [29], are $\alpha1 = -1 \times 10^{-6}$ 1/K and $\alpha2 = \alpha3 = 4 \times 10^{-5}$ 1/K. A room temperature of 20 °C was considered, giving a 105 °C temperature drop from the 125 °C curing and glass transition temperature.

A FE analysis similar to the one explained in Section 3.2 *Finite element analysis.* was used to calculate the residual thermal stresses at the free edge of the substrate laminate when no binding is applied and when a $[\pm45]_s$ binding is applied. Fig. 9 shows the numerical results obtained for the through-thickness stresses S_{33} and S_{13} in global coordinates (x, y, z) at the free edge of the substrate laminate.

As shown in Fig. 9, the application of the $[\pm45]_s$ additive binding is not affecting the S_{13} stress in either AP or QI laminate. However, the binding applies some compressive stress in the z-direction, reaching about −22 MPa at the top and bottom surfaces of the free-edges.

This indicates that the binding layers are not only constraining the relative movement of the layers by introducing through-thickness constraints but also providing small compressive stress, which may further suppress any potential free-edge delamination.

4. Experiments

4.1. Materials

The material used for the substrate laminate manufacturing was Hexply IM7/913 prepreg, provided by Hexcel, with a fibre areal weight of 130 g/m^2. For the binding, thin-ply prepreg from SK Chemicals with the commercial name of Skyflex USN020 with TC33 carbon fibres and K51 epoxy resin was used. Both resin systems were cured at 125 °C according to their curing cycle provided by the manufacturers. The material properties for the applied prepregs are shown in Table 1.

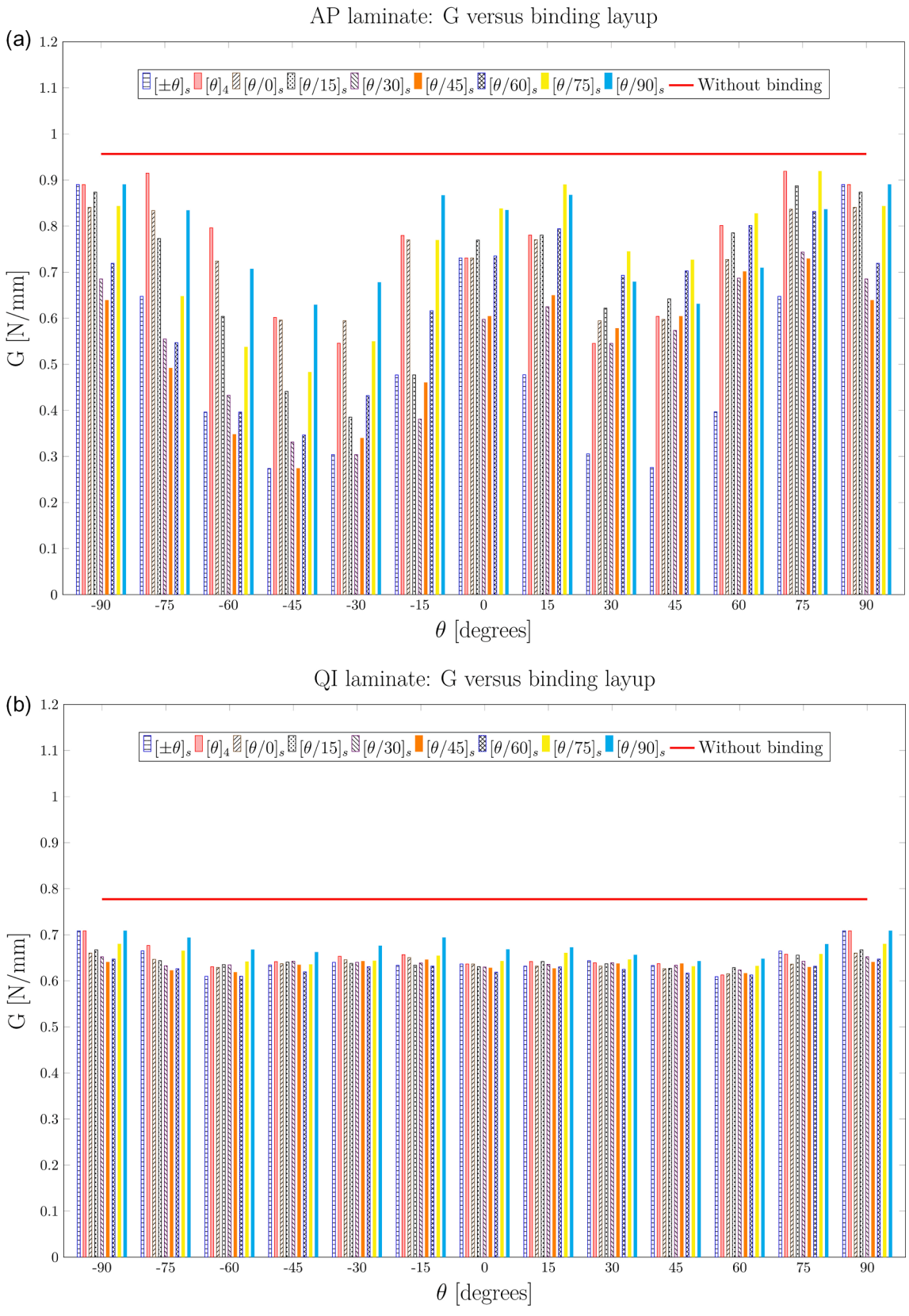

Fig. 6. Highest energy release rate values of the AP and QI substrates treated with different binding layups of $[\pm\theta]_s$, $[\theta]_4$ and $[\theta/\varphi]_s$ at their critical interfaces compared against the energy release rate of the substrates with no binding. (a) AP substrate with a pre-crack of 4.5 mm at interface 1 or 7. (b) QI substrate with a pre-crack of 4.5 mm at interface 3 or 5. (For interpretation of the references to colour in this figure legend, the reader is referred to the web version of this article.)

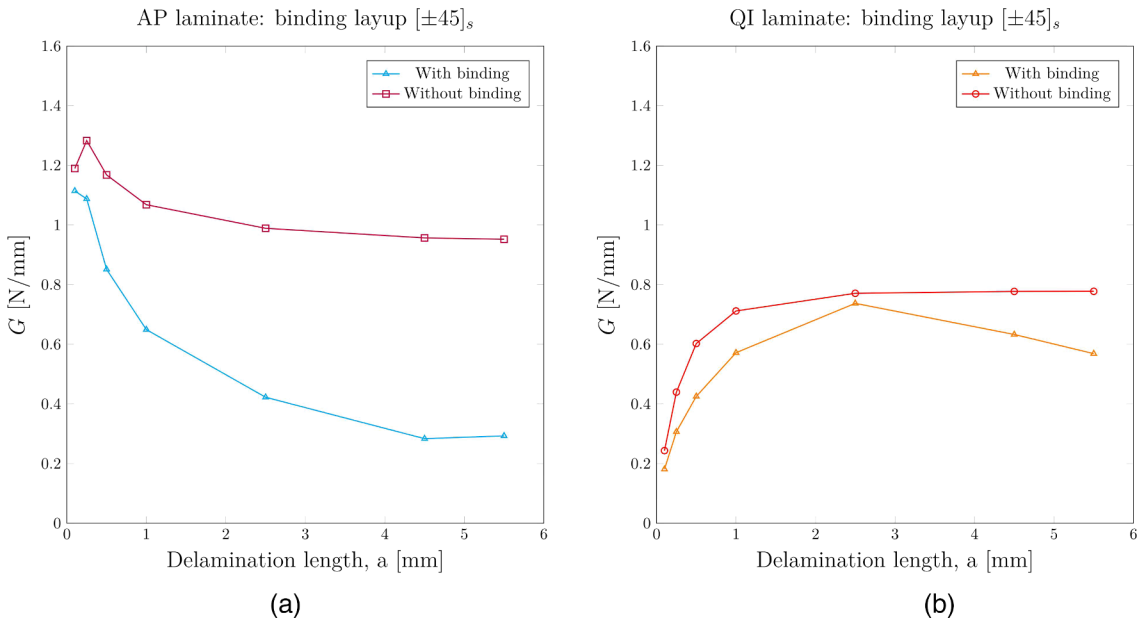

Fig. 7. Energy release rate versus crack length for laminates with and without additive binding. (a) AP laminate with delamination at interface 1, (b) QI laminate with delamination at interface 3. (For interpretation of the references to colour in this figure legend, the reader is referred to the web version of this article.)

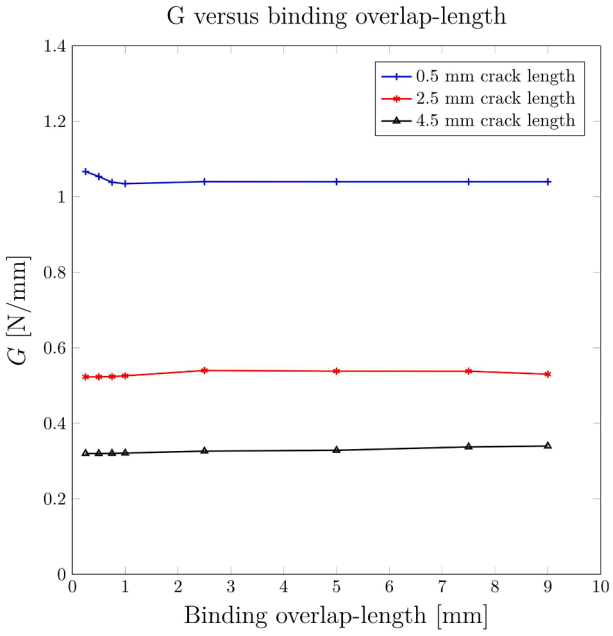

Fig. 8. Energy release rate versus the overlap-length of a $[\pm 45]_s$ additive binding applied to the AP substrate laminate with 0.5, 2.5 and 4.5 mm delamination lengths at the critical interface. (For interpretation of the references to colour in this figure legend, the reader is referred to the web version of this article.)

4.2. Specimens manufacture

The specimens manufactured and tested in this study were parallel-edge end-tabbed tensile specimens. The dimensions were 200 mm long with 120 mm free from end-tabs, 20 mm wide, and an average measured thickness of 2.12 mm, which gives a measured cured ply thickness of IM7/913 to be 0.13 mm, equal to the nominal thickness reported by the manufacturer.

The manufacture of the substrate laminates was similar to the conventional processes for curing standard prepregs. First, 300 mm by 300 mm IM7/913 composite plates were cured in an autoclave at the recommended temperature and pressure cycle for the Hexcel 913 epoxy resin, 60 min at 125 °C and 7 bars. Then, the specimens were cut from the plates using a water-jet bench tool. Next, End-tabs were bonded to the substrate laminate using a two-component Araldite 2014-2 glue and were let to cure at room temperature for at least 24 h.

After the tensile samples were end-tabbed, additive bindings were applied to the edge of the substrates and then cured following the K51 epoxy resin curing cycle, 30 min dwell at 80 °C and 90 min at 125 °C with a pressure of 5 bars. The binding plies were cut from a flat, uncured prepreg roll, stacked up to build a 120 mm long and 12 mm wide laminate. The nominal ply thickness for this material is 0.03 mm [29]. The 12 mm width was selected so that the overlap-length on both top and bottom surfaces is 5 mm, considering approximately 2 mm for the substrate laminate thickness. The manufacture, placement and vacuum bagging of the bindings are schematically shown in Fig. 10 and explained as follows:

(i) Plies were laid upon a flat plate to build the stacking sequences of $[\pm 45_s]$ or $[0]_4$ depending on the applied binding layup.
(ii) The middle of each binding was placed along the substrate mid-plane at the free edges and then folded carefully over the substrate's top and bottom surfaces, as illustrated in Fig. 10a.
(iii) A plastic release film was wrapped around the free length of the substrate laminate, as shown in Fig. 10b.
(iv) Batches of 7 or 8 specimens were placed in a fully sealed vacuum bag. A breather cloth was used between the vacuum bag and the samples to ensure the vacuum applied an evenly distributed pressure to the free length of all substrates. Fig. 10c shows schematically the specimens prepared for the second autoclave curing stage.
(v) The vacuum bag containing the batch of specimens was put in an autoclave, and the bindings were cured according to the binding prepreg curing cycle.

It is worth noting that all specimens were cured according to the manufacturer's curing cycle. Moreover, the curing temperature of the substrate laminate and the binding were the same (125 °C). Hence, it is not expected that a second curing cycle on the substrate laminates with bindings would have a great impact on the samples.

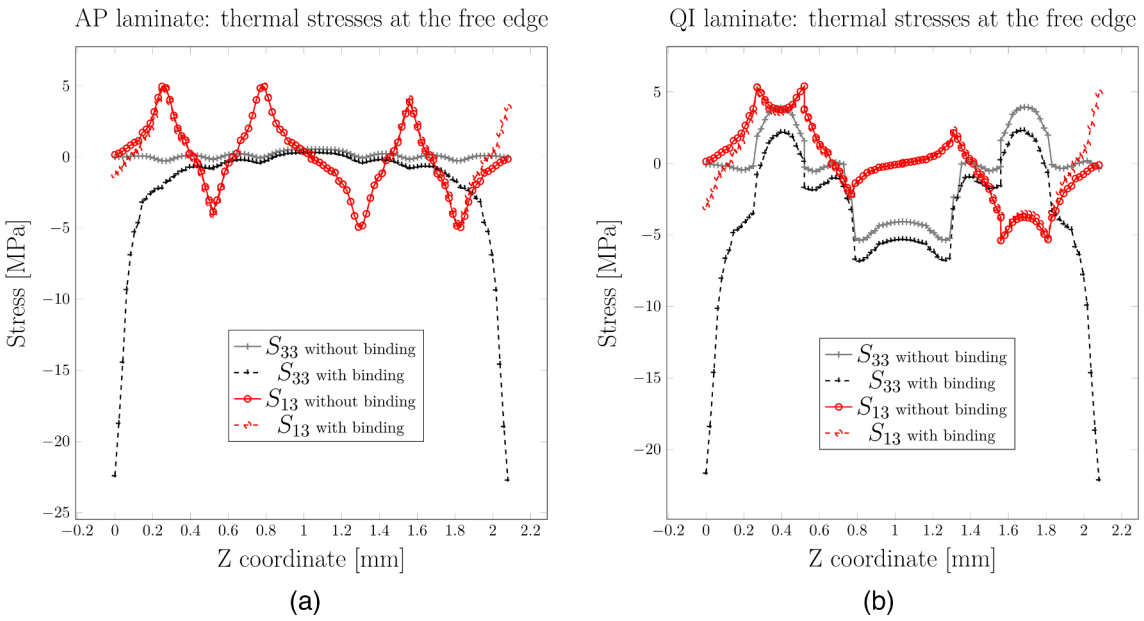

Fig. 9. Thermal stresses S_{33} and S_{13} in global coordinates at the free edges of the substrate laminates without and then with a $[\pm 45]_s$ binding applied. (a) AP laminate, (b) QI laminate. (For interpretation of the references to colour in this figure legend, the reader is referred to the web version of this article.)

Table 1
UD prepreg properties for IM7/913 and TC33/K51.

Prepreg	E_{11} (GPa)	$E_{22} = E_{33}$(GPa)	$\nu_{12} = \nu_{13}$	ν_{23}	$G_{12} = G_{13}$(GPa)	G_{23} (GPa)	*Strain to failure* ε_{11}* (%)	*vf (%)*
IM7/913	159.87[a]	11.38[b]	0.32[b]	0.45[b]	5.2[b]	3.9[b]	1.6[a]	57.4[a]
TC33/K51	95.3[c]	6.1[c]	0.3[c]	0.45[c]	2.47[c]	3.9[d]	1.5[c]	39[c]

[a] Data by the manufacturer. E_{11} calculated using the rule of mixtures.
[b] Assumed to be equal to that of IM7/8552 found in [30].
[c] [29].
[d] No data was found in the literature. Several numerical simulations were performed, showing a negligible effect of G_{23} on energy release rate values. Therefore, it was assumed to be equal to that of IM7/913.

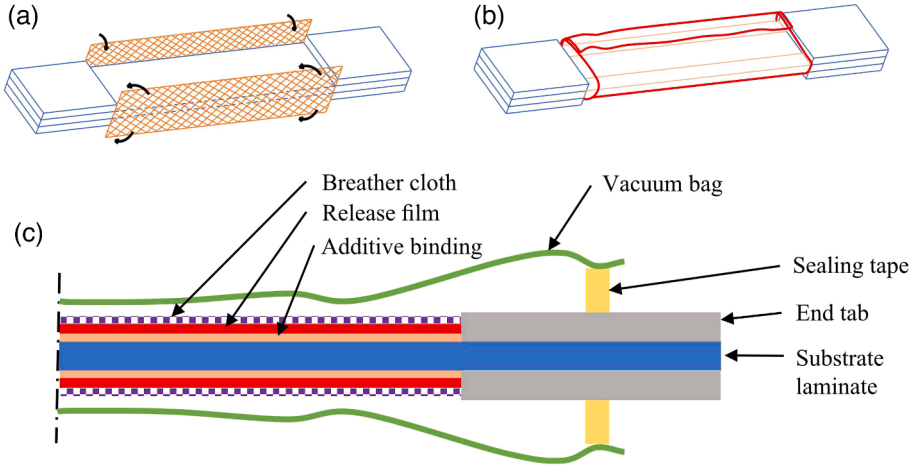

Fig. 10. Binding manufacture and application to the substrate laminate's free edges, (a) folding the binding laminate over the free edge of the substrate, (b) wrapping the release film around the binding and substrate laminates, (c) the substrate with the binding inside the vacuum bag. (For interpretation of the references to colour in this figure legend, the reader is referred to the web version of this article.)

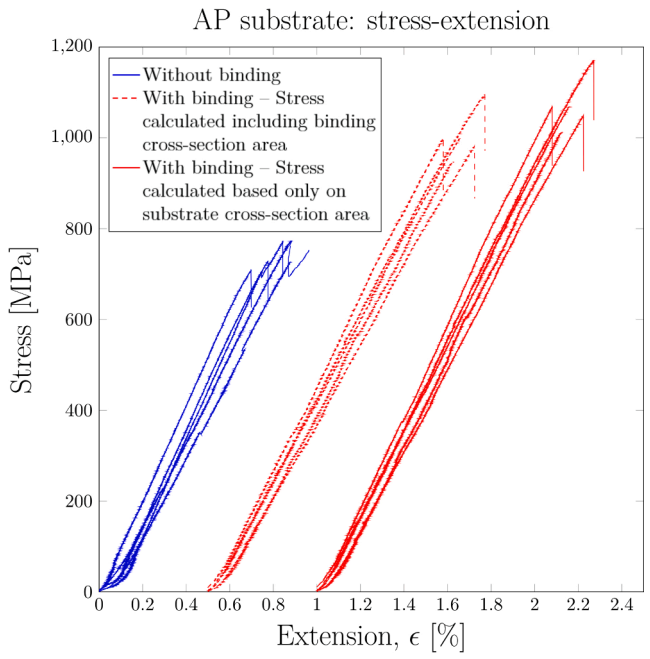

Fig. 11. Stress-extension experimental results for the AP substrates without any binding and with $[\pm 45]_s$ binding. (For interpretation of the references to colour in this figure legend, the reader is referred to the web version of this article.)

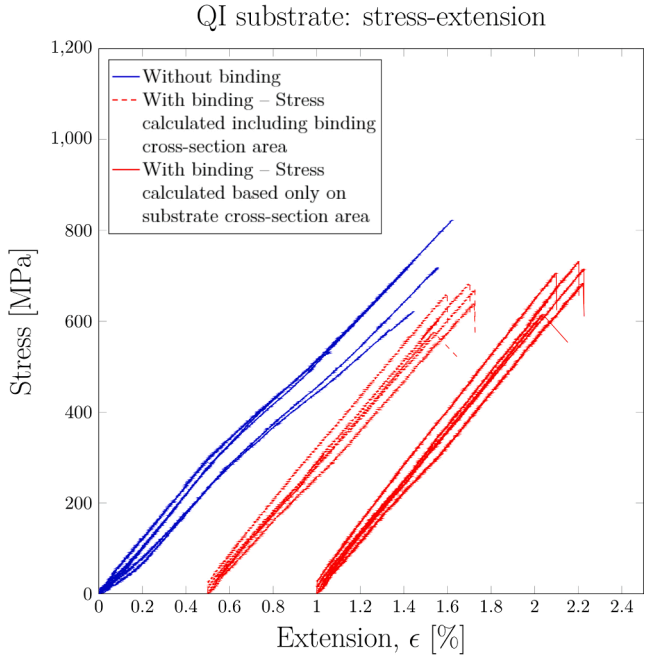

Fig. 12. Stress-extension experimental results for the QI substrates without any binding and with $[\pm 45]_s$ binding. (For interpretation of the references to colour in this figure legend, the reader is referred to the web version of this article.)

4.3. Experimental results

The mechanical testing was conducted under quasi-static displacement-control tensile loading at 1 mm/min rate. A computer-controlled

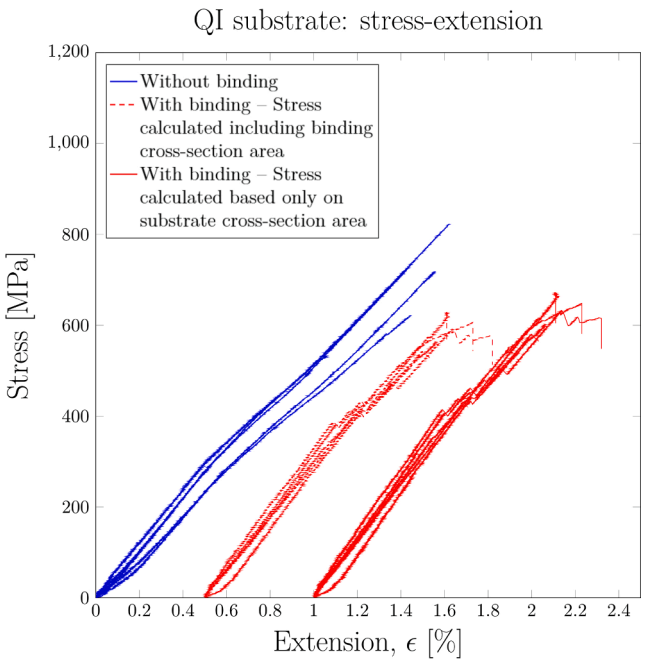

Fig. 13. Stress-extension experimental results for the AP substrates without any binding and with $[0]_4$ binding. (For interpretation of the references to colour in this figure legend, the reader is referred to the web version of this article.)

Instron Electromechanical 5969 50 kN universal testing machine with mechanical wedge grips was used to apply the load. An Instron 2663-821 video extensometer system was used for measuring the axial extension of the specimens. Five repetition samples per layup configuration were tested until failure.

For calculating the average applied stress to the specimens without binding, the force measured by the load cell was divided by the cross-section area of each specimen. The width of all specimens was measured separately at 3 points along the length and then averaged. The nominal ply thickness of 0.13 mm was used for calculating the total thickness of the substrate laminates.

Two cross-sectional areas were used to calculate the stress in the samples with binding, and two stress values were calculated: (1) substrate cross-sectional area as explained above plus binding's nominal cross-sectional area, and (2) substrate cross-sectional only. It is believed that both stress definitions provide useful information. This is because a different binding overlap length does not affect the value of G and consequently would not change the failure load as shown in Fig. 8, i.e. a binding with 2 mm overlap-length would have the same failure force with a smaller binding cross-section area. Hence, it is useful to show the stresses only based on the substrates cross-sectional area.

It is worth mentioning that the cross-section of the binding is less than 7% of the substrate's cross-sectional area and would not change the graphs significantly.

The stress-extension results for samples with and without binding are shown in Figs. 11, 12 and 13 for the AP laminates and the QI laminates with $[\pm 45_s]$ and $[0]_4$ bindings, respectively. The cases with binding are plotted with an offset of 0.5% strain to make the comparison clearer. Table 2 presents the load direction engineering modulus, maximum force, stress based only on substrate cross-section area, and strain at failure of the AP and QI laminates with and without binding.

The strain and force at failure are taken as the points where the first

significant drop of the load is seen, defining the point when the laminate cannot withhold the load anymore. For the case without binding, the AP laminates show an average value of 0.8%, 733.21 MPa and 30.78 kN for strain, stress, and load at the failure point, respectively. The QI laminates show similar average values of 721.59 MPa and 30.36 kN for stress and load at failure, but due to lower axial stiffness, the failure strain is 1.49%, almost double that of the AP laminates.

The AP laminates with $[\pm 45]_s$ additive bindings show a significant increase in their strain, stress, and force at failure. The average strain at failure was 1.19%, indicating a significant 49% increase compared to the 0.80% failure strain of the AP laminates without binding. A similar 47% increase is observed in the average maximum force, from 30.78 to 45.21 kN. On the contrary, the QI laminates show a slight reduction of about 4% in the average values of failure stress and force and a small increase in the stiffness of the laminate when $[\pm 45]_s$ bindings are applied, reducing the strain at failure 22% from 1.49% strain to 1.16% strain. The $[0]_4$ bindings applied to the QI substrate seem to cause more noticeable reductions in the failure stress and force, although it increased the stiffness of the laminates too, reducing the strain at failure 29% from 1.49% strain to 1.05% strain. The obtained experimental results are discussed in the next section.

For calculating the engineering modulus of the laminates, the slope of a straight line between two points on the stress-extension graphs at 0.2% and 0.4% extension were used for each specimen and then averaged for each group.

It is worth mentioning that after inspection of all failed specimens, no debond between the binding and the substrate was identified at points away from the main failure points, so it can be concluded that the additive binding does not tend to debond from the substrate laminate. This is aligned with the very low energy release rate values calculated for assumed cracks between the binding and the substrate, as explained in Section 3.2 *Finite element analysis.*

5. Discussion

This section aims to explain how the binding suppressed the damage modes triggered by the free-edges, e.g. free-edge delamination and matrix cracking, whereas other failure modes are not greatly affected.

5.1. Failure analysis of the AP substrate.

Xu and Wisnom showed that $[(20_2/-20_2)_2]_s$ AP laminates under tension fail shortly after initiation of the free-edge delamination [25]. Equation 1 and the FE slice modelling results can be used to find the free-edge delamination onset strain of the AP laminates. From the FE analysis, the mixed-mode ratio is found to be equal to one, $(G_{II} + G_{III})/(G_I + G_{II} + G_{III}) = 1$, for the AP laminates. Therefore, the fracture toughness, G_c, is assumed to be equal to pure mode-II fracture toughness. No data was found for the fracture toughness values of the IM7/913, so the value of fracture toughness G_{Ic} and G_{IIc}, which are known to be mostly matrix dependant, were taken as $G_{Ic} = 0.25$ N/mm and $G_{IIc} = 1.08$ N/mm, estimated from E-Glass/913 prepreg in [31]. Additionally, G_{IIIc} was assumed equal to G_{IIc} as per the common practice [30]. Introducing this G_c value in Equation 1, the free-edge delamination onset strain in the AP laminates is calculated to be 0.98%. For calculating E^* in Eq. (1), two complete and symmetrical delaminations are assumed between the outer 20_2 layers and the inner layers. The FE analysis provides a free-edge delamination onset strain of 0.92%, calculated with a pre-crack length of 0.25 mm as the value of G is maximum at this delamination length as shown in Fig. 7a.

The analytical and FE free-edge delamination onset strain predictions are higher than the observed average failure strain of 0.8% for

Table 2
Maximum force, stress and strain at failure for AP and QI laminates.

Specimen	Load direction engineering modulus [GPa] (CV %)	Maximum force [kN] (CV%)	Failure stress [MPa] (CV %)	Failure strain [abs.%] (CV %)
AP laminate without binding	100.47 (8.23)	30.78 (3.39)	733.21 (3.25)	0.80 (9.76)
AP laminate with [±45]s binding	95.6 (5.04)	45.21 (5.00)	1077.21 (4.95)	1.19 (6.85)
QI laminate without binding	56.07 (6.61)	30.36 (9.72)	721.59 (9.85)	1.49 (6.04))
QI laminate with [±45]s binding	57.82 (6.51)	29.03 (6.55)	690.37 (6.54)	1.16 (7.33)
QI laminate with [0]4 binding	66.70 (3.30)	26.35 (6.00)	627.03 (5.77)	1.05 (15.75)

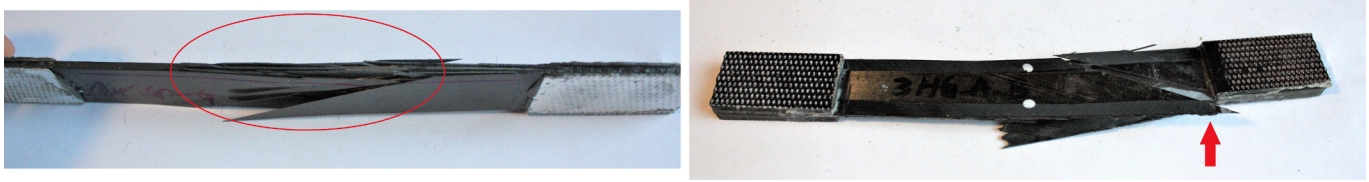

Fig. 14. AP laminates after failure, (a) without binding, (b) with binding. (For interpretation of the references to colour in this figure legend, the reader is referred to the web version of this article.)

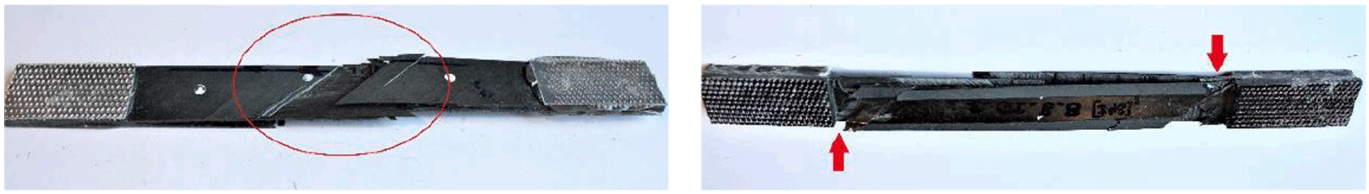

Fig. 15. QI laminates after failure, (a) without binding, (b) with $[\pm 45]_s$ bindings. (For interpretation of the references to colour in this figure legend, the reader is referred to the web version of this article.)

the AP laminates without binding. This could be partially explained as AP laminates do not fail only by free-edge delamination but due to an interaction between free-edge delamination and splitting of the plies. When those splits and delaminations propagated, they joined through the thickness, and the surface ply peeled off, as clearly shown in Fig. 14a and described by Xu and Wisnom in [25].

Similarly, O'Brien observed that the experimental onset strain of free-edge delamination occurs at strains lower than the strain values predicted in Equation 1 and, therefore, proposed an empirical modification to the same equation to include 2 in the denominator of the equation rather than 4 [10]. He justified this change based on the presence of zig-zag and asymmetric delamination in reality.

The possibility of failure modes other than free-edge delamination was studied using Classical Laminate Theory. The fibre, transverse, and shear direction stresses in all ±20 layers at 0.80% applied axial strain are calculated to be equal to 907.5, −75.0 and ±62.1 MPa, respectively. All these values are significantly lower than the material's estimated tensile strength in fibre direction (2723 MPa) [32], transverse compression strength (286 MPa) [33], as well as shear strength (88.3 MPa), estimated from the E-glass/913 shear strength in [34]. This indicates that the free-edge delamination initiated the failure process of the AP laminates without binding. This is also confirmed by examining the failed specimens shown in Fig. 14. AP laminates after failure. (a) Without binding, (b) with binding, where a red circle indicates extensive free-edge delamination and separation of the layers.

For the AP laminates with binding, the failure strain is increased 49%, from 0.8% for those without binding to 1.19%. As the laminate is treated with the binding, O'Brien's analytical technique is not applicable to calculate the free-edge delamination onset strain. The FE results presented in Fig. 7a indicate a significant reduction in the energy release rate for delamination growth, suggesting that the delamination growth would be stable, unlike the AP laminates without binding. For delamination lengths of about 4 mm, the energy release rate is estimated to be 0.42 N/mm at 1.19% strain, where the G approaches an asymptote. This value is significantly lower than the mode-II fracture toughness, and therefore, no catastrophic free-edge delamination growth is expected.

The fibre, transverse and shear direction stress values in all ± 20 layers at 1.19% axial strain are calculated to be equal to 1350, −111.6 and ±92.4 MPa, respectively. While fibre and transverse direction stresses are far below the strength values, the shear direction stress is above the shear strength value of 88.3 MPa. This suggests that ±20 layers are most likely to break due to shear at this axial strain. In the absence of other layers in this substrate, e.g. 0 layers, failure of the ±20 layers leads to the whole laminate final failure. Fig. 14(b) indicates one of the AP samples after its failure point. No edge delamination is detectable, and the failure is relatively localised (highlighted with a red arrow) with cracks along the fibre, suggesting a shear failure mode.

It is to be noted that the selection of a $[\pm 45]_s$ binding layup indicated by the FE modelling did stop the free-edge delamination. This shows the capabilities of the FE modelling approach for choosing an appropriate binding layup. Further experiments on other binding layups can help to build a richer set of experimental results and is suggested by the authors as an interesting future research.

5.2. Failure analysis of the QI substrate

From the detailed experiments in [35], we know that the final failure of the QI laminates occurs when the 0 layers fail due to fibre failure. Therefore, the final failure process of the QI laminates without binding is not controlled by free-edge delamination. Nonetheless, free-edge delamination and matrix cracking can cause stiffness reduction.

From the FE analysis, the mixed-mode ratio for the free-edge delamination in the QI laminates is found to be $(G_{II} + G_{III})/(G_I + G_{II} + G_{III}) = 0.6$. Using the BK-law [36] with an exponent value 1, the fracture toughness, G_c, is estimated to be equal to 0.748 N/mm, using $G_{Ic} = 0.25$ N/mm and $G_{IIc} = 1.08$ N/mm from [31].The free-edge delamination onset strain is calculated to be 1.12% using Equation 1, whereas E^* was calculated assuming that QI laminates completely and symmetrically delaminate at the two critical interfaces. The G values from FE analysis shown in Fig. 7 b, for the case without binding, are small for short delamination lengths and increase gradually to an asymptotic value by which the free-edge delamination onset strain is calculated to be 0.98%. Predictions from both Equation 1 and FE are significantly higher than 0.55% extension around which the slope of the initial linear elastic stress-extension graphs changes indicating stiffness reduction. This suggests the possibility of initiation of other failure modes, e.g. matrix cracking in the off-axis 90 and ±45 layers as the first mode of damage in the QI layup.

Based on Classical Laminate Theory, 90 layers transverse direction stress at a strain of 0.63% is higher than their transverse strength (88.3 MPa). This is close to 0.55% axial strain at which the stress-extension curves of the QI laminates without binding start to deviate from the linear-elastic response. This indicates that matrix cracking is likely to initiate first and induce free-edge delamination at higher strains.

Fig. 15a shows both QI samples without binding after failure. Transverse cracks in the off-axis layers and delamination are clear.

Introduction of the $[\pm 45]_s$ bindings to the QI laminates resulted in a slight 4% reduction in their final failure load and a 22% reduction in the final failure strain. The similarity in the failure load is mainly because the final failure process of the QI laminates is not dominated by free-edge delamination, and introducing the bindings does not have a significant impact on the 0 layers fibre failure load. The reduction in the failure strain is caused by a 23% increase in the secant load direction engineering modulus of the laminates between the origin and the final failure point. The binding suppresses the in-plane transverse and interlaminar damage arising from the free-edges, and no change of slope is distinguishable in the stress-extension graph. Comparing the stress-extension graphs in Fig. 12 b indicates that the laminates with binding show an almost perfect linear elastic response up to their final failure point. Those without binding show some nonlinearity caused by possible matrix cracking and free-edge delamination. The slight 4% reduction in the final load failure is believed to be due to the stress concentration caused by the bindings at the end-tabs, as shown in Fig. 15(b) with a red arrow. It is expected that this reduction of failure load could be avoided if the binding was first applied to the full length of the QI substrates without end-tabs, and then end-tabs were bonded to the binding.

The results obtained from $[0]_4$ bindings show a reduction of 12% in

the load-bearing capacity of the laminate and a 30% reduction in the failure strain. Similar to the $[\pm 45]_s$ bindings, the reduction in the failure load is assumed to be due to stress concentration caused by the binding at the end tab, and as $[0]_4$ laminate has higher stiffness along the load direction. This has caused higher stress concentration at the end tabs and resulted in a lower failure load. Also, the reduction in the failure strain is due to a 17% increase in the secant engineering modulus of the samples between the origin and the final failure point. Additionally, the load-extension graphs of the QI specimens with $[0]_4$ bindings showed a clear sign of damage and nonlinearity around 0.6–0.8% extension that suggests this binding laminate was not successful in suppressing the damages initiating from the free edges

6. Conclusion

The idea of using additive bindings as an effective technique to suppress free-edge delamination is presented. Finally, the concluding points of this study are mentioned below:

- Using additive bindings at the free edges on laminates susceptible to free-edge delamination under axial loading can significantly enhance their failure load and strain. In the angle-ply laminate $[(20_2/-20_2)_2]_s$ studied in this paper, the failure load and failure strain were increased by 47% and 49%, respectively.
- The use of this technique can suppress other modes of damage arising at the free edges, e.g. matrix cracking. In the quasi-isotropic layup studied in this paper, the nonlinearity of the stress-extension curve was eliminated, indicating the matrix cracking and free-edge delamination in the off-axis layers were successfully suppressed.
- The $[\pm 45]_s$ additive bindings do not affect other failure modes. This is deemed to be because of their small quantity compared to the main substrate and relatively low stiffness in the load direction. For instance, the final failure stress stayed almost unchanged in the quasi-isotropic substrate, indicating that the final failure process dominated by 0-degree layer fibre failure was not affected by the bindings. This is particularly good news for testing and characterisation purposes, suggesting that binding is mainly eliminating the damages initiated by the free-edges, and other failure modes are not affected.
- Improvement of the binding manufacturing methods could be further explored for avoiding the introduction of stress concentration at the binding termination point. For example, longer bindings covered by the end-tab could potentially resolve this issue.
- This technique could be used to suppress free-edge delamination in real structures or composite laminate coupon samples for material characterisation testing.

CRediT authorship contribution statement

Miguel Ubago Torres: Conceptualization, Methodology, Software, Validation, Formal analysis, Investigation, Data curation, Writing – original draft, Writing – review & editing, Visualization, Project administration. **Meisam Jalalvand:** Conceptualization, Methodology, Software, Resources, Writing – review & editing, Supervision, Funding acquisition.

Declaration of Competing Interest

The authors declare that they have no known competing financial interests or personal relationships that could have appeared to influence the work reported in this paper.

References

[1] Pagano NJ, Pipes RB. Some observations on the interlaminar strength of composite laminates. Int J Mech Sci 1973;15(8):679–88. https://doi.org/10.1016/0020-7403(73)90099-4.

[2] Pipes RB, Pagano NJ. Interlaminar stresses in composite laminates under uniform axial extension. J Compos Mater 1970;4(4):538–48. https://doi.org/10.1177/002199837000400409.

[3] Rybicki EF. Approximate three-dimensional solutions for symmetric laminates under inplane loading*. J Compos Mater 1971;5(3):354–60. https://doi.org/10.1177/002199837100500305.

[4] Isakson G, Levy A. Finite-element analysis of interlaminar shear in fibrous composites. J Compos Mater 1971;5(2):273–6. https://doi.org/10.1177/002199837100500215.

[5] Pipes RB. Moiré analysis of the interlaminar shear edge effect in laminated composites. J Compos Mater 1971;5(2):255–9. https://doi.org/10.1177/002199837100500211.

[6] Wang ASD, Crossman FW. Some new results on edge effect in symmetric composite laminates. J Compos Mater 1977;11(1):92–106. https://doi.org/10.1177/002199837701100110.

[7] Hsu PW, Herakovich CT. Edge effects in angle-ply composite laminates*. J Compos Mater 1977;11(4):422–8. https://doi.org/10.1177/002199837701100405.

[8] Wang JTS, Dickson JN. Interlaminar stresses in symmetric composite laminates. J Compos Mater 1978;12(4):390–402. https://doi.org/10.1177/002199837801200404.

[9] Rybicki EF, Schmueser DW, Fox J. An energy release rate approach for stable crack growth in the free-edge delamination problem. J Compos Mater 1977;11(4):470–87. https://doi.org/10.1177/002199837701100409.

[10] O'Brien T. Characterization of delamination onset and growth in a composite laminate. In: Damage Compos Mater Basic Mech Accumul, Toler Charact, 100 Barr Harbor Drive. PO Box, C700, West Conshohocken, PA: 19428-2959: ASTM International; 1982. p. 140–67. https://doi.org/10.1520/STP34325S.

[11] Ss WANG. Fracture mechanics for delamination problems in composite materials. Stud Appl Mech 1984:369–83. https://doi.org/10.1016/B978-0-444-42169-2.50029-2.

[12] Ye L. Role of matrix resin in delamination onset and growth in composite laminates. Compos Sci Technol 1988;33:257–77. https://doi.org/10.1016/0266-3538(88)90043-7.

[13] Chan WS, Wang ASD. Effects of a 90° ply on matrix cracks and edge delamination in composite laminates. Compos Sci Technol 1990;38(2):143–57. https://doi.org/10.1016/0266-3538(90)90003-N.

[14] Krieger RB. An Adhesive Interleaf to Reduce Stress Concentrations Between Plys of Structural Composites. Adhes. 12, vol. 32, Dordrecht: Springer Netherlands; 1988. p. 159–65. https://doi.org/10.1007/978-94-009-1349-3_10.

[15] Pagano NJ, Lackman LM. Prevention of delamination of composite laminates. AIAA J 1975;13(3):399–401. https://doi.org/10.2514/3.49713.

[16] Chan W, Ochoa O. Suppression of edge delamination in composite laminates by terminating a critical ply near the edges. Reston, Virginia: American Institute of Aeronautics and Astronautics; 1988. https://doi.org/10.2514/6.1988-2257.

[17] Lee E, Chan W. Delamination arrestment by discretizing the critical ply in a laminate. Reston, Virginia: American Institute of Aeronautics and Astronautics; 1989. https://doi.org/10.2514/6.1989-1403.

[18] Mignery L, Tan T, Sun C. The use of stitching to suppress delamination in laminated composites. delamination debonding mater, 100 Barr Harbor Drive, PO Box C700, West Conshohocken, PA 19428-2959: ASTM International; 1985. p. 371-371–15. https://doi.org/10.1520/STP36315S.

[19] Howard WE, Gossard T, Jones RM. Composite laminate free-edge reinforcement with U-shaped caps. Part I - Stress analysis. AIAA J 1989;27(5):610–6. https://doi.org/10.2514/3.10152.

[20] Howard WE, Gossard T, Jones RM. Composite laminate free-edge reinforcement with U-shaped caps Part 11: Theoretical-experimental correlation. AIAA J 1989;27(5):617–23. https://doi.org/10.2514/3.48818.

[21] Chuaqui TRC, Sebastian E, Sahadevan V, Rhead AT, Butler R. Edge treatment of short beam shear tests for improved assessment of structural strength. Compos Part A Appl Sci Manuf 2020;137:105991. https://doi.org/10.1016/j.compositesa.2020.105991. In press.

[22] Chuaqui TRC, Nielsen MWD, Colton J, Butler R, Rhead AT. Effects of ply angle and blocking on open-hole tensile strength of composite laminates: a design and certification perspective. Compos Part B Eng 2021;207:108582. https://doi.org/10.1016/j.compositesb.2020.108582.

[23] Krueger R. Virtual crack closure technique: History, approach, and applications. Appl Mech Rev 2004;57:109–43. https://doi.org/10.1115/1.1595677.

[24] Tsai S, Sihn S, Kim R. Thin ply composites. In: 46th AIAA/ASME/ASCE/AHS/ASC Struct. Struct. Dyn. Mater. Conf. 4. Reston, Virigina: American Institute of Aeronautics and Astronautics; 2005. p. 2555–9. https://doi.org/10.2514/6.2005-2005.

[25] Xu X, Wisnom MR. An experimental and numerical investigation of the interaction between splits and edge delaminations in [+20m/-20m] ns carbon/epoxy laminates. In: ECCM 2012 – compos venice, proc 15th Eur conf compos mater; 2012.

[26] O'Brien T. Mixed-mode strain-energy-release rate effects on edge delamination of composites. Eff. Defects Compos. Mater., 100 Barr Harbor Drive, PO Box C700, West Conshohocken, PA 19428-2959: ASTM International; 1983. p. 125-125–18. https://doi.org/10.1520/STP30201S.

[27] Jiang W-G, Henshall JL. Analysis of composite laminate beams using coupling cross-section finite element method. Appl Math Mech 2006;27(12):1709–18. https://doi.org/10.1007/s10483-006-1213-z.
[28] Krueger R. Finite element analysis of composite joint configurations with gaps and overlaps, NASA/CR-2014-218284; 2014. <https://ntrs.nasa.gov/archive/nasa/casi.ntrs.nasa.gov/20140010076.pdf>.
[29] Rev T. Exploiting thin-ply materials to establish controlled failure in carbon composites. University of Bristol 2020. https://research-information.bris.ac.uk/ws/portalfiles/portal/241708717/THESIS_FULL_TR_POSTVIVA_final_unsigned.pdf.
[30] Krueger R. Development and Application of benchmark examples for mode II static delamination propagation and fatigue growth predictions. 2011. <https://ntrs.nasa.gov/search.jsp?R=20110023248>.
[31] Petrossian Z, Wisnom MR. Prediction of delamination initiation and growth from discontinuous plies using interface elements. Compos Part A Appl Sci Manuf 1998; 29(5-6):503–15. https://doi.org/10.1016/S1359-835X(97)00134-6.
[32] Hexcel. HexTow® IM7 Carbon Fiber. Hexcel Corp Accessed 20 Novemb 2018 2018; 000:1–2.
[33] Guedes RM, Vaz MA, Ferreira FJ, Morais JL. Overview of coupon testing of an IM7/8552 composite required to characterize high-energy impact dynamic material models. Sci Eng Compos Mater 2005.
[34] Wisnom MR, Jones MI. A comparison between interlaminar and in-plane shear strength of unidirectional glass fibre-epoxy. Adv Compos Lett 1994;3: 096369359400300. https://doi.org/10.1177/096369359400300205.
[35] Wisnom MR, Khan B, Hallett SR. Size effects in unnotched tensile strength of unidirectional and quasi-isotropic carbon/epoxy composites. Compos Struct 2008; 84(1):21–8. https://doi.org/10.1016/j.compstruct.2007.06.002.
[36] Benzeggagh ML, Kenane M. Measurement of mixed-mode delamination fracture toughness of unidirectional glass/epoxy composites with mixed-mode bending apparatus. Compos Sci Technol 1996;56(4):439–49. https://doi.org/10.1016/0266-3538(96)00005-X.